Journal of Marine Science and Application (2022) 21: 95-103
https://doi.org/10.1007/s11804-022-00304-8

RESEARCH ARTICLE

Two-Phase Fatigue Life Prediction of Small-Scale Welded Specimens Based on the Experimental Results

Ivana Gledić[1], Antonio Mikulić[1] and Joško Parunov[1]

Received: 16 Mar 2022 / Accepted: 08 Oct 2022

Abstract

The study aims to calibrate parameters of two-phase fatigue prediction model based on the results of the small-scale fatigue test experiments for zero stress ratio and without residual stresses, and then to investigate their applicability for different stress ratios and in the presence of residual stresses. Total fatigue life using the two-phase model consists of crack initiation phase, calculated by strain-life approach, and crack propagation phase, calculated by fracture mechanic's approach. Calibration of the fatigue parameters is performed for each phase by fitting numerical to the experimental results. Comparative analysis of calculated and measured fatigue lives is then conducted for different stress ratios, in both stress-relieved and as-welded conditions. Given that calculation parameters are calibrated for the basic case, uncertainty of predictions is large, showing that application of the method for real-life complex marine structures is challenging.

Keywords Two-phase fatigue model; Crack initiation; Crack propagation; Stress ratio; Residual stress; Initial crack size

1 Introduction

Fatigue and crack growth in ships and offshore structures are a highly uncertain and complex phenomenon (Dong et al., 2022). Fatigue life of ship structural details can be predicted using one of main fatigue design models: stress-life (S-N), the local strain-life (ε-N), the fatigue crack growth (da/dN-ΔK) and the two-phase model (TPM) (Lassen and Recho, 2006; Fatemi et al., 2001). The last model incorporates the local strain-life (crack initiation stage) and fatigue crack growth (crack propagation stage) model. When added together the total fatigue life is obtained providing a whole history of crack propagation. TPM is commonly used by the industry for fatigue life prediction of welded structural details subjected to the cyclic load. It is well known, however that accuracy of the fatigue life prediction highly depends on the parameters used for the TPM, and it is recommended to determine these parameters on case-by-case basis. Even in such a case when parameters are determined for one specific configuration, it is questionable if they will be equally valid for different stress ratios and different level of residual stresses.

Different procedures have been developed for fatigue life prediction based on databases of the fatigue behaviour of welded structures and following theoretical research and experiments (Fricke and Petershagen, 1992; Fricke, 2003). Cui (2002) made a review of existing models for fatigue life prediction, where it was concluded that most used approach is the S-N approach. Huang et al. (2014) analysed fatigue reliability of complex welded structures and fatigue damage was quantified by the S-N approach. Kodvanj et al. (2021) obtained fatigue lives and stress concentration factor (SCF) for small-scale specimens experimentally. These results of SCF were then compared with the finite element method following a correlation analysis between actual and predicted crack location. S-N approach is also adopted by classification societies for ship structural design (IACS 2014)

Article Highlights

- Fatigue life of small-scale welded specimens is investigated by the two-phase model;
- Parameters of the model are calibrated based on the fatigue experiments for without residual stresses and for zero stress ratio;
- Total fatigue lives for different residual stresses and stress ratios can be predicted with reasonable accuracy;
- Considerable uncertainty is expected in the practical application of the method.

✉ Joško Parunov
jparunov@fsb.hr

[1] Faculty of Mechanical Engineering and Naval Architecture, University of Zagreb, Zagreb 10 000, Croatia

Chen (2016) studied crack initiation by low-cycle fatigue (LCF) in design of stop hole for repair of ship cracks. LCF is considered as primary failure modes for oil tankers and FPSO ships caused by repeating liquid cargo loading and unloading (DNVGL, 2015). Possibility of LCF occurrence in damaged ship is investigated by Gledić et al. (2019).

Fracture mechanics (FM) has been applied to determine the fatigue life of cracked components (Garbatov and Guedes Soares, 2004) and for inspection planning (Chen et al., 2011). It is also suitable for reliability assessment of a stiffened panel subjected to correlated crack growth (Feng et al., 2012) and for fatigue assessment of corroded deck longitudinals of tanker (Parunov et al., 2013). Committee on Fatigue and Fracture of the International Ships and Offshore Structures Congress (Ås et al., 2018) provides recent developments in fatigue assessment methods. They pointed out that even though some new methods and theories in field of fatigue and fracture emerged, fatigue crack growth approach based on the theory of FM is still the most valuable tool for preventing fatigue failure of the ship. Ship classification rules provides guidelines on the practical application of crack propagation using linear elastic FM (Bureau Veritas, 2016). FM is used for crack propagation in damaged ship as a part of the emergency response procedure (Gledić et al., 2021).

TPM approach was originally proposed by Socie et al. (1979) as a simple model for calculation of total fatigue life by combining LCF concept and fracture mechanics concepts. Dong et al. (2018) made further progress were TPM model was applied to predict total fatigue lives of experimentally tested notched specimens.

Welded joints add considerable complexity in fatigue life calculation comparing to the non-welded structural component. Fatigue life of welded structures is influenced by weld geometry (weld toe radius and weld toe angle) and material properties. However, it is found that residual stress has the highest impact on fatigue life (Fatemi et al., 2001). Dexter and Pilarski (2002) confirmed considerable influence of residual stresses by a series of experiments on welded stiffened panels, showing that crack propagation is reduced because of compressive residual stresses between stiffeners. Božić et al. (2018) presented a method for predicting fatigue crack propagation in welded stiffened panels accounting for the effects of residual stresses, achieving good agreement with experimental results.

The aim of the present study is to calibrate parameters of TPM based on the results of the small-scale fatigue test experiments and then to investigate their applicability for different stress ratios (R) and in the presence of residual stresses σ_{res}. Experiments used for calibration are performed by Friedrich (2020), where fatigue lives of crack initiation phase and crack propagation phase are presented for different stress ratios for multi-layer K-butt weld. Furthermore, results are presented separately for as-welded condition with residual stresses, and for the case when residual stresses due to welding are relieved.

The analysis is performed in a way that parameters of TPM are calibrated based on the experimental results for $R = 0$ and for residual stress-relieved condition. After that, the analysis with the same parameters is performed to investigate agreement with the experiments in the presence of the residual stresses. The analysis is further extended for different stress ratios in both as-welded and stress-relieved conditions.

The paper is organized in the following way. In the next section TPM is described. After that, experiments performed by Friedrich (2020) are briefly recapitulated for the sake of the completeness of the paper. Finite element analysis is described in section 4. Calibration of the parameters is described in the sections 5 and 6, together with the comparison of predictions and experiments for different stress ratios with and without residual stresses. The paper ends with discussion and corresponding conclusions.

2 Two-phase fatigue model

Fatigue life is defined as number of loading cycles until failure is reached, i.e., total number of cycles N_t. In this study calculation of fatigue life is based on TPM (Lassen and Recho, 2006), mathematically described as follows

$$N_t = N_i + N_p \tag{1}$$

where N_i is the number of cycles until crack initiation and N_p is the number of cycles of crack propagation until failure occurs. The key point of TPM is the continuation of the two stages of fatigue, i.e., proper definition of the crack initiation that is not clearly defined and represents a challenging task.

In the first phase of TPM, number of cycles to crack initiation N_i is calculated by a local stress-strain approach modelled by the Coffin-Manson equation with Morrow's mean stress correction:

$$\frac{\Delta\varepsilon_{\text{loc}}}{2} = \frac{\left(\sigma'_f - \sigma_m\right)}{E}\left(2N_i\right)^b + \varepsilon'_f\left(2N_i\right)^c \tag{2}$$

where $\Delta\varepsilon_{\text{loc}}$ is the non-linear local strain range and σ_m is the local mean stress at weld toe. E is the Young's modulus of elasticity. The parameters b and c are the fatigue strength and ductility exponents, and σ'_f and ε'_f are the fatigue strength and ductility coefficients, respectively.

Local strain range, $\Delta\varepsilon_{\text{loc}}$, is calculated by the combination of the Neuber's Rule,

$$\Delta\varepsilon_{\text{loc}}\Delta\sigma_{\text{loc}} = \frac{\left(\Delta\sigma_n \cdot \text{SCF}\right)^2}{E} \tag{3}$$

and Ramberg-Osgood equation,

$$\Delta\varepsilon_{\mathrm{loc}} = \frac{\Delta\sigma_{\mathrm{loc}}{}^{2}}{E} + 2\Delta\sigma_{\mathrm{loc}}\left(\frac{\Delta\sigma_{\mathrm{loc}}}{2K'}\right)^{\frac{1}{n'}} \tag{4}$$

where: K' and n' are the cyclic strength coefficient and strain hardening exponent, respectively. $\Delta\sigma_n$ is nominal stress range and SCF is the linear stress concentration factor. $\Delta\sigma_{\mathrm{loc}}$ is the non-linear local stress range.

The solution of this σ-ε loop can be found by different iterative process. Herein the Newton-Raphson method is used. Once the $\Delta\varepsilon_{\mathrm{loc}}$ is calculated, N_i can also be obtained from Eq. 2 using an iterative procedure.

Second phase of TPM is a crack propagation phase where crack propagates from initial crack depth a_0 to crack of critical depth a_c. This phase is described by the Paris-Erdogan law:

$$\frac{\mathrm{d}a}{\mathrm{d}N} = C(\Delta K)^m, \Delta K > \Delta K_0 \tag{5}$$

where C and m are treated as material parameters for a given stress ratio R and environmental condition, ΔK is the stress intensity factor range (SIFR) at the crack tip corresponding to the applied nominal stress range $\Delta\sigma_n$ and ΔK_0 is threshold stress intensity factor range below which fatigue crack growth (or corrosion fatigue crack growth) does not occur. It should be noted that Eq. 5 does not have the capability to explain many experimental phenomena such as stress ratio effect, load sequence effect and unstable fracture effect. Modified forms of Paris equation are proposed to cover these effects (Fatemi et al., 2001).

The SIFR can be written as follows:

$$\Delta K = K_{\max} - K_{\min} \tag{6}$$

$$\Delta K = \Delta\sigma_n F(a)\sqrt{\pi a} \tag{7}$$

The number of cycles to reach given critical crack depth a_c is calculated by numerical integration of the Paris-Erdogan law as follows:

$$N_p = \int_{a_o}^{a_c} \frac{\mathrm{d}a}{C\left(\Delta\sigma_n F(a)\sqrt{\pi a}\right)^m} \tag{8}$$

where a_0 is the initial crack depth and a_c is the final or crack depth at which fracture will occur. $F(a)$ is the geometry function which depends on geometry of crack, namely type and size of crack. From Eq. 8, one should be aware that N_p is sensitive to a_0 and that a_0 also defines the N_i.

For fatigue assessments the following equation applies (British Standard, 2005):

$$F(a) = f_w \cdot M_m \cdot M_k \cdot \mathrm{SCF} \tag{9}$$

where f_w is the finite width correction factor, in case of a long surface flaws in plates $f_w = 1$; M_m is the stress intensity magnification factor due to membrane loading. In this study only membrane part of the solution is calculated because it is assumed that bending stress is caused only by geometrical eccentricity of the joint and not by forced stress on the structure. Sub-functions (M_m, M_b) from Eq. 9 can be found in British Standard (2005). These sub-functions include the effects of the curved shape of the crack, the finite thickness and finite width of the plate. When a flaw or crack is situated in a region of local stress concentration, i. e. weld toe, stress intensity is changed. This change is quantified through stress gradient factor M_k. In case of the small cracks M_k will coincide with the SCF at the weld toe. For as-welded joints under membrane loading equations are provided in British Standard (2005).

3 Experiment overview

Friedrich (2020) conducted the experiment to predict the fatigue life of a multilayer K-butt weld between two steel plates of 10- and 25 mm thickness as shown in Figure 1, for different stress ratios and for two different conditions: stress-relieved and as-welded. The experiment specimens are made of steel grade S355J2C+N welded by metal active gas. Detailed data about specimen preparation can be found in Friedrich (2020).

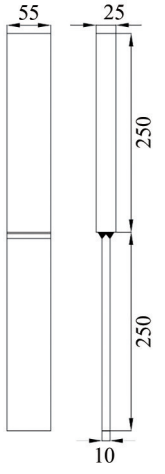

Figure 1 Specimen preparation (Friedrich, 2020)

Static mechanical properties of the 10 mm plate were determined by tensile tests: yield strength R_{eH} = 394 MPa; tensile strength R_m = 524 MPa; Young's modulus E = 201 GPa. The tests were performed on a 200 kN resonance testing machine for four different cases i.e. four different load ratios R: R = 0 (tension), $R = -\infty$ (compression), $R = -1$ and $R = -3$ (alternating stress). The test is run until complete rupture of the specimen.

In experiments, residual stresses were measured using two techniques, namely X-ray diffraction and hole-drilling (Friedrich, 2020) showing differences in results, where the hole drilling measurements resulted in larger residual stresses compared to the X-ray diffraction measurements. The residual stress measurements showed tensile residual stresses transversal to the weld at the centre of the specimen and compressive stresses at the edges. Expectedly, the highest value of residual stress is at the weld toe, and it decreases towards the longitudinal end of the specimen. Estimated mean value of tensile residual stresses at the weld toe is around 150 MPa and it is taken into consideration when performing calculation for as-welded condition. Residual stress distribution is shown in Figure 2 in Friedrich (2020) and not repeated herein. A clarification is necessary regarding the fact that the small-width specimen is not conducive to the retention of residual stress. Namely, as reported by Friedrich (2020), it was confirmed by the numerical analysis that the residual stresses persist even in the small-width specimen.

There is no prescribed value of initial crack size a_0 (Ås et al., 2018). It can only be assumed based on the data provided in literature. Lassen and Recho (2006) suggested an initial crack size between 0.01 mm and 0.05 mm. However, this assumption must be taken with a caution because the crack of this small size is too close to microstructural features of structural steel (Ås et al., 2018).

Friedrich (2020) assumed initial crack size of 2 mm wide, based on the engineering judgement, arguing that this length could reliably be detected in the performed fatigue tests, even by visual observation. It is further assumed in the present study that crack shape is elliptical and therefore that crack depth is half-size of the detected crack width, i.e. about 1 mm. Therefore, that value of initial crack depth is assumed herein.

The crack location is also important for the fatigue life prediction. From Figure 4 in Friedrich (2020), the macroscopic crack initiation occurs in the mid-length along the weld toe. The crack location at mid-length of the weld toe is expected, as that is the region of the highest tensile residual stresses.

4 Finite element analysis

Prior to calculation of crack initiation period N_i, fine mesh finite element analysis (FEA) was performed to find SCF (Figure 2). The model accounts for measured misalignment $e = 0,33$ mm and angular distortion $\varphi = 0.33°$ (Friedrich, 2020) which is a consequence of welding. This step was necessary for determination of SCF at hot spot according to (Bureau Veritas, 2016; Kodvanj et al., 2021; Hobbacher, 2016).

$$\mathrm{SCF}_{HS} = \frac{\Delta\sigma_{HS}}{\Delta\sigma_n} = 1.19 \tag{10}$$

with $\Delta\sigma_{HS}$ as hot spot stress obtained by FEA and $\Delta\sigma_n$ as nominal stress range.

The toe of the weld, i.e. a local notch, is the localized geometric feature which causes stress concentration. The local notch induces a non-linear stress peak in the vicinity of the weld. Presence of the weld therefore leads to the increase of the SCF:

$$\mathrm{SCF} = K_w \mathrm{SCF}_{HS} = 2.08 \tag{11}$$

where K_w is the notch factor, which is tightly dependent on the weld toe geometry, i.e. the toe angle θ and the weld toe radius ρ. Weld toe angle $\theta = 40°$ is obtained from FEM and weld toe radius is assumed to be 1 mm. K_w is calculated by equation provided in Lassen and Recho (2006) and reads 1.75.

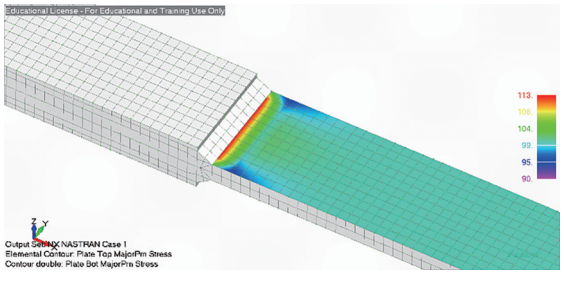

Figure 2 FEM of K-Butt joint and hot spot stress $\Delta\sigma_{HS}$

5 Crack initiation

5.1 Calibration of crack initiation parameters for $R = 0$ without residual stresses

As the starting point for their optimization, the cyclic mechanical properties and parameters in Coffin-Manson equation were taken from Jovičić et al. (2015) (Table 1). The parameters were obtained from the uniaxial tension–compression fatigue tests of the S355J2+N material, which is the same material as in the present study. All values from Table 1 are within the range of expected values and the upper and lower limits given in Lassen and Recho (2006) and Fatemi et al. (2001).

Analysis of parameters for $R = 0$ showed that two parameters from Table 1 have comparably larger influence on overall results, namely fatigue strength coefficient σ'_f and fatigue ductility coefficient ε'_f. σ'_f is effective when low stress range is applied, while ε'_f is more pronounced for high stress range. After the adjustment of these two coefficients (Table 2), excellent agreement is achieved between experimental curve and calculated results, which is shown in Figure 3.

Table 1 Cyclic mechanical properties of S233J2+N material (Jovičić at al., 2015)

Parameter	Value
Strength coefficient K' (MPa)	720.94
Strain hardening exponent n'	0.125 8
Fatigue strength exponent b	−0.052 1
Fatigue ductility exponent c	−0.398 7
Fatigue strength coefficient σ'_f (MPa)	525.31
Fatigue ductility coefficient ε'_f	0.066 2

Table 2 Optimized parameters for Coffin-Manson equation

Parameter	Optimized value
Fatigue strength coefficient σ'_f (MPa)	220
Fatigue ductility coefficient ε'_f	0.15

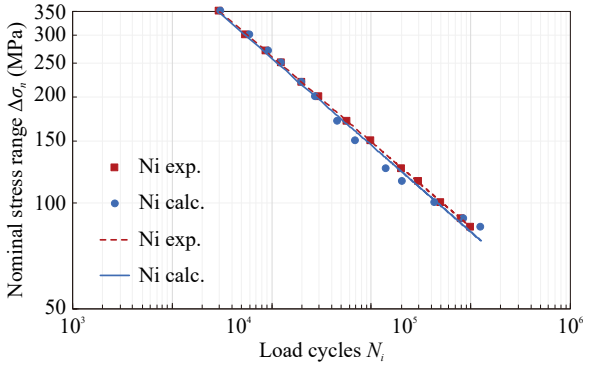

Figure 3 Calibration of crack initiation parameters for $R = 0$ in stress-relived condition ($\sigma_{res} = 0$)

Even though there are no prescribed values or set of limits for coefficients σ'_f and ε'_f, when optimized values are compared with values available from literature and from Table 1, fatigue ductility coefficient is within expected range, while the fatigue strength coefficient σ'_f is found unexpectedly low after optimization.

5.2 Validation of crack initiation parameters for different stress ratios and residual stresses

With established crack initiation parameters, next step is to examine their adequacy for different stress ratios for as-welded and stress relieved conditions.

Residual stress effect on fatigue crack initiation is calculated by the Coffin-Manson Eq. 2 with Morrow's mean stress correction. Comparison of the results for $R = 0$ in Figure 4 shows slight decrease of the fatigue life in the presence of the residual stresses with similar trend for calculations and experiments.

One can notice that there is a difference in presentation of results (Figures 3 and 4) for the same case, $R = 0$ in stress-relieved condition. The reason is that experimental results

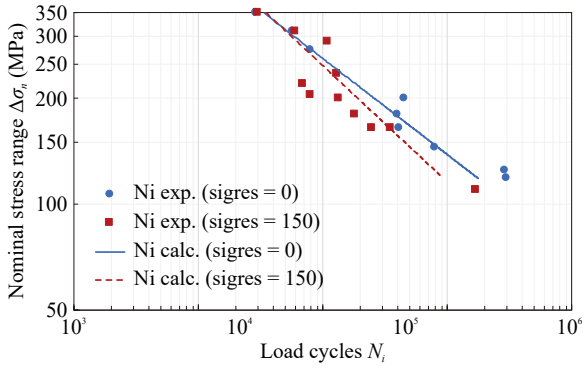

Figure 4 Crack initiation for stress ratio $R = 0$, $\sigma_{res} = 0$ and for $\sigma_{res} = 150$ MPa

in Figure 3 are presented as the continuous regression line to calibrate crack initiation parameters, while Figure 4 shows calibrated crack initiation curve through discrete, measured experimental data points.

For the case of $R = -1$, stress relieved results are slightly shifted to the left but still parallel with experiment data, while as-welded results fairly overlap (Figure 5).

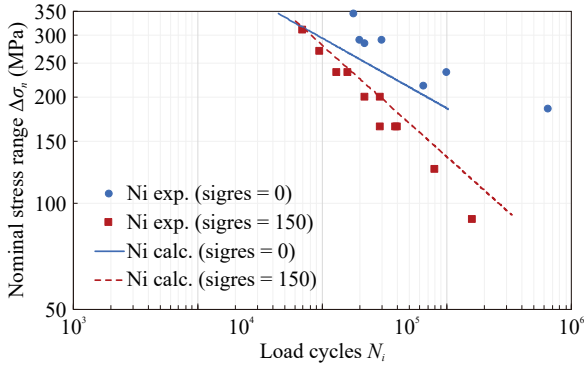

Figure 5 Crack initiation for stress ratio $R = -1$, $\sigma_{res} = 0$ and for $\sigma_{res} = 150$ MPa

It should be noted that results for stress ratio $R = -3$ were not compared for stress-relieved condition because results of the experiment were close and S-N curve could not be determined by linear regression. Figure 6 shows comparison of the results for as-welded condition for $R = -3$ and $R = -\infty$. In former case a good agreement of calculated results is obtained, while for $R = -\infty$ results are shifted to the right.

6 Crack propagation

6.1 Calibration of crack propagation parameters for $R = 0$ without residual stresses

As a starting point for optimization of the parameters in

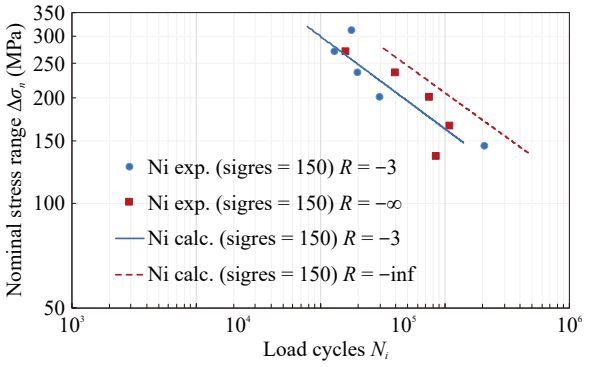

Figure 6 Crack initiation for stress ratio $R = -3$ and $R = -\infty$, $\sigma_{res} = 150$ MPa

Paris-Erdogan law, a crack growth parameter C is assumed to be equal to a mean value proposed by Lassen and Recho (2006) (Table 3). Given that crack growth parameter m is a slope of the crack growth cure, its value is set to be equal to a slope of the experiment crack propagation curve for $R = 0$ in stress-relieved condition (Table 3), i.e., $m = 2.873$. As elaborated in Section 2, crack depth of 1 mm is assumed as the initial crack size.

Table 3 Initial parameters C, m and a_0

Parameter	Initial value
Crack growth parameter C (mm/(MPa·mm$^{1/2}$)^m)	$1.85 \cdot 10^{-13}$
Crack growth parameter, m	2.873
Initial crack size a_0 (mm)	1

The results for this set of values showed that even though there is an overlap of calculated and measured results, a further optimization of the parameters is necessary.

The optimization is conducted in a same way as it was for the crack initiation, for stress ratio $R = 0$ and for stress-relieved state. As shown in Figure 7 optimization resulted in a fair overlap between experiment and results from crack growth calculation, where optimized crack growth coefficient C reads $6.5 \cdot 10^{-13}$ mm/(MPa·mm$^{1/2}$)^m.

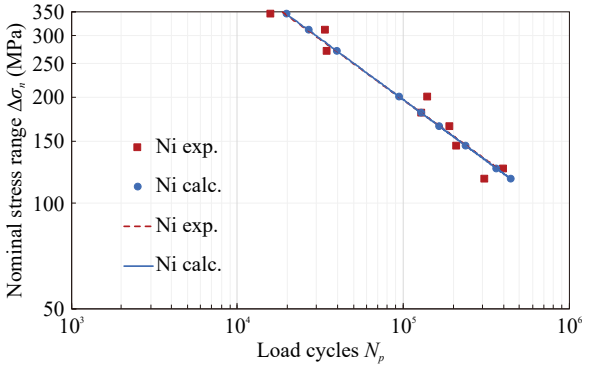

Figure 7 Calibration of crack propagation parameters for $R = 0$ in stress-relived condition ($\sigma_{res} = 0$)

As previously mentioned, definition of the initial crack size is uncertain. To further investigate this effect on optimized parameters, two more initial crack depths are considered equal to 0.5 and 1.5 mm. It was found that for each initial crack size and same crack growth parameter m, there is a corresponding value of parameter C (Figure 8). For different combinations of C and a_0, overlap as in the Figure 7 is achieved.

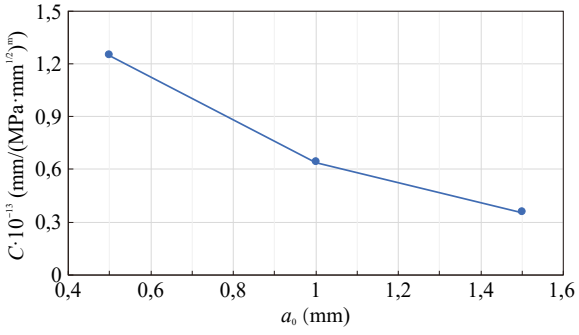

Figure 8 Relation of a_0 and crack growth parameter C for $m = 2.873$

6.2 Validation of crack propagation parameters for different stress ratios and residual stresses

It is assumed herein that only positive part of the applied stress range contributes to the crack growth while during the negative part of the loading cycle there is no crack growth, i.e., the crack remains closed (Fatemi et al., 2001; Almar-Naes et al., 1985).

Stress ratio is calculated as follows,

$$R = \frac{\sigma_{\min}}{\sigma_{\max}} \tag{12}$$

while nominal stress range $\Delta\sigma_n$ is defined as

$$\Delta\sigma_n = \sigma_{\max} - \sigma_{\min} \tag{13}$$

where $\sigma_{\min}$ and $\sigma_{\max}$ are minimum and maximum of the applied nominal stress range $\Delta\sigma_n$.

If only positive part of the applied nominal stress is considered, then maximum $\sigma_{\max}$ is equal to:

$$\sigma_{\max} = \frac{\Delta\sigma_n}{1 - R} \tag{14}$$

For crack propagation analysis, the residual stress for as welded condition can be considered by superposition to the applied stress (Fatemi et al., 2001),

$$\sigma_{\max} = \frac{\Delta\sigma_n}{1 - R} + \sigma_{\text{res}} \tag{15}$$

$$\sigma_{\min} = R \cdot \sigma_{\max} + \sigma_{\text{res}} \tag{16}$$

Figure 9 shows comparison of results for $R = 0$ with- and without residual stresses. As in both cases whole load cycle is tensile, there is no difference in calculated fatigue life. Experimental results indicate slightly higher fatigue life for the case with the residual stresses.

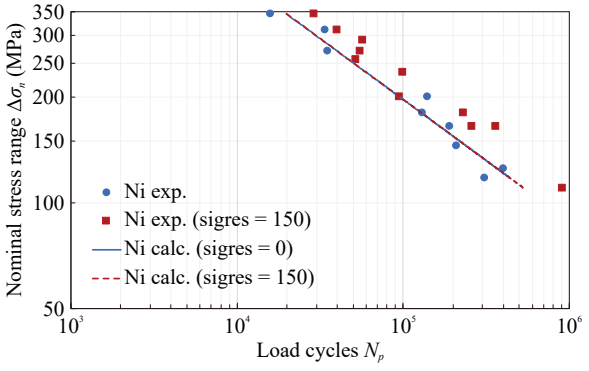

Figure 9 Crack propagation for stress ratio $R = 0$, $\sigma_{res} = 0$ and $\sigma_{res} = 150$ MPa

Regarding the difference between results shown in Figure 7 and Figure 9, case of $R = 0$ and stress-relieved condition, the same explanation as for the initiation phase applies (see Section 5.2).

Figure 10 shows comparison of calculated and measured fatigue lives for $R = -1$, where underestimation of measured fatigue life by calculations may be noticed.

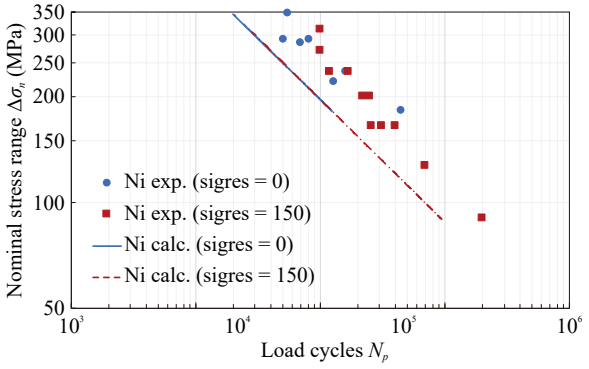

Figure 10 Crack propagation for stress ratio $R = -1$, $\sigma_{res} = 0$ and $\sigma_{res} = 150$ MPa

For stress ratio $R = -3$ results were not compared for stress-relieved condition because results of the experiment were too close and S-N curve was not determined by linear regression. Figure 11 shows comparison of the results for as-welded condition for $R = -3$ and $R = -\infty$. In both cases calculated results underestimate experimentally determined fatigue lives.

7 Discussion

As mentioned in Section 2, fatigue life, i.e., total number of cycles calculated by TPM is a sum of crack initiation and crack propagation cycles. Results of total fatigue life are plotted in Figures 12 & 13 for as-welded and stress-relieved condition, respectively. Closer inspection of plotted results indicates that in as-welded condition, Figure 12, calculated curves for $R = 0$ and $R = -1$ overlap well with those obtained experimentally. Calculated results for $R = -3$ slightly underestimate experimental fatigue lives, but with same trend. In case of $R = -\infty$, curve slope of calculated results is lower compared to the experiment.

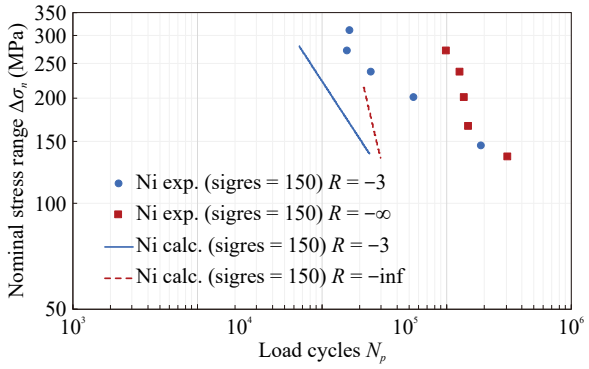

Figure 11 Crack propagation for stress ratio $R = -3$ and $R = -\infty$, $\sigma_{res} = 150$ MPa

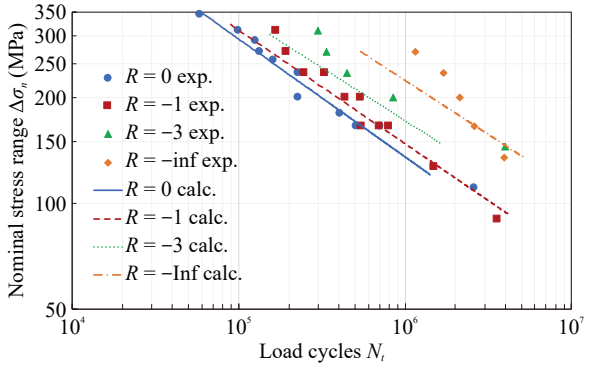

Figure 12 Total fatigue life for as-welded condition

The effect of the stress ratio R is different for as-weld and stress-relieved conditions. In as-welded condition tensile residual stress reduces the effect of the load ratio. Consequently, S-N curves lie close together (Figure 12). The influence of stress ratio is more obvious in stress-relieved condition with curves which are much more apart (Figure 13).

Throughout this work the assumption is made that only positive part of the applied stress range contributes to crack propagation, which means that during the lower part of the loading cycle crack remains closed and does not contribute to the crack growth. However, Fatemi et al. (2001) emphasize that compression cycle may also be important for fatigue crack growth, in which case they suggested Walker relationship and Foreman equation.

It is recognized that one of the key issues in the applica-

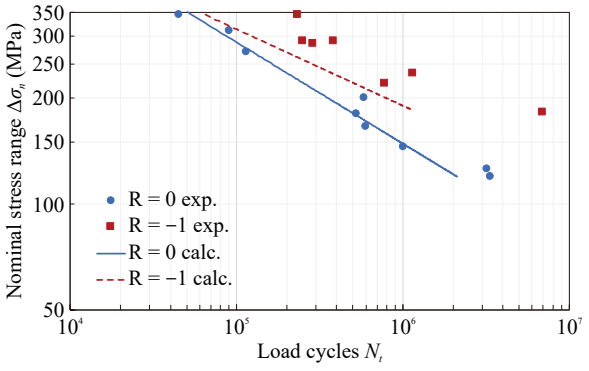

Figure 13 Total fatigue life for stress-relieved condition

tion of TPM is definition of the initial crack size a_0 , representing the boundary between two phases. It is also known that the initial defects always exist in engineering marine structures, especially ships. If so, the fatigue may be considered as purely a crack propagation problem and other improved crack growth rate methods, such as Unified Fatigue Life Prediction (UFLP) equation may be employed (Cui et al., 2011). UFLP requires a given loading history and the accumulated crack length is calculated on a cycle-by-cycle basis. This could accurately account for many loading effects such as mean stress effect, load sequence effect and structural efects such as notch effect and size effect. As a future work, it is recommended to attempt employing UFLP for solving the present problem.

8 Conclusions

Fatigue life of small-scale welded specimens is investigated using the two-phase approach. Parameters of crack initiation and crack propagation phases are calibrated based on fatigue experiments for stress-relieved condition and for stress ratio $R = 0$. It was found that the results are mostly affected by fatigue strength coefficient σ'_f and fatigue ductility coefficient ε'_f . Different combinations of initial crack size a_0 and crack growth parameter C may be employed to fit measured results with calculations using two-phase model.

Total fatigue lives for different stress ratios and residual stresses can be predicted with reasonable accuracy using fatigue parameters determined for $R = 0$ in stress-relieved condition. Better agreement of calculations and measurements is achieved for cases of high tensile stresses at stress notch, i.e., for higher R and for as-welded condition. Given that calculation parameters are calibrated by the measurements, uncertainties in predictions are large, indicating that considerable uncertainty in predicted fatigue life is expected in the practical application of the method for the real-life complex marine structures.

References

Almar-Næss A (1985) Fatigue handbook-offshore steel structures. Tapir Publishers, Norway

Ås SK, Branner K, Chi BK, den Besten JH, Dong P, Garbatov Y, Lillemäe I, lindstrom P, Loirenco de Souza M, Parmentier G, Quéméner Y, Rizzo CM, Rörup J, Vhanmane S, Villavicencio R, Wang F & Yuan Y (2018) Committee III.2: Fatigue and Fracture. Proceedings of the 20th International Ship and Offshore Structures Congress (ISSC). Vol. 1: 441-547. CRC Press. https://doi.org/10.3233/978-1-61499-862-4-441

Božić Ž, Schmauder S, Wolf H (2018) The effect of residual stresses on fatigue crack propagation in welded stiffened panels. Engineering Failure Analysis 84: 346-357. https://doi.org/10.1016/j.engfailanal.2017.09.001

British Standard (2005) Guide to methods for assessing the acceptability of flaws in metallic structures (BS 7910). BSI, London, United Kingdom

Bureau V (2016) Guidelines for Fatigue Assessment of Steel Ships and Offshore Units (NI 611 DT R00 E). Bureau Veritas. Neuilly sur Seine Cedex, France

Chen NZ (2016) A stop-hole method for marine and offshore structures. International Journal of Fatigue 88: 49-57. https://doi.org/10.1016/j.ijfatigue.2016.03.010

Chen NZ, Guedes Soares C, Wang G (2011) Palmgren-Miner's rule and fracture mechanics-based inspection planning. Engineering Fracture Mechanics 78: 3166-3182. https://doi.org/10.1016/j.engfracmech.2011.08.002

Cui W (2002) A state-of-the-art review on fatigue life prediction methods for metal structures. Journal of Marine Science and Technology 7: 43-56. https://doi.org/10.1007/s007730200012

Cui W, Wang F, Huang X (2011) A unified fatigue life prediction method for marine structures, Marine Structures 24(2): 153-181. https://doi.org/10.1016/j.marstruc.2011.02.007

Det Norske Veritas Germanischer Lloyd (DNVGL) (2015) Fatigue Assessment of Ship Structure. Classification Notes, No. 30. 7. DNV-GL AS

Dexter RJ, Pilarski, PJ W (2002) Crack propagation in welded stiffened panels. Journal of Constructional Steel Research 58: 1081-1102. https://doi.org/10.1016/j.ijfatigue.2003.08.006

Dong Y, Garbatov Y, Guedes Soares C (2018) A two-phase approach to estimate fatigue crack initiation and propagation lives of notched structural components. International Journal of Fatigue 116: 523-534 https://doi.org/10.1016/j.ijfatigue.2018.06.049

Dong Y, Garbatov Y, Guedes Soares C (2022) Review on uncertainties in fatigue loads and fatigue life of ships and offshore structures. Ocean Eng. https://doi.org/10.1016/j.oceaneng.2022.112514

Fatemi A, Fuchs HO, Stephens RI, Stephens RR (2001) Metal fatigue in engineering. Second Edition, John Wiley & Sons, Inc. Hoboken, New Jersey, United States of America

Feng GQ, Garbatov Y, Guedes Soares C (2012) Probabilistic model of the growth of correlated cracks in stiffened panel. Engineering Fracture Mechanics 84: 83-95. https://doi.org/10.1016/j.engfracmech.2012.01.008

Fricke W, Petershagen H (1992) Detail design of welded ship structures based on hot-spot stresses. Proceedings of the Practical Design of Ships and Mobile Units, J. B. Caldwell and G. Ward, Elsevier Science Limited, Vol. 2: 1087-1100

Fricke W (2003) Fatigue analysis of welded joints: state of development. Marine Structures 16(3): 185-200. https://doi.org/10.1016/S0951-8339(02)00075-8

Friedrich N (2020) Experimental investigation on the influence of

welding residual stresses on fatigue for two different weld geometries. Fatigue Fracture of Engineering Materials and Structures 43: 2715–2730. https://doi.org/10.1111/ffe.13339

Garbatov Y, Guedes Soares C (2004). Influence of steel strength on the fatigue reliability of welded structural components. International Journal of Fatigue 26(7): 753-762. https://doi.org/10.1016/j.ijfatigue.2003.10.020

Gledić I, Mikulić A, Parunov J (2021) Improvement of the Ship Emergency Response Procedure in Case of Collision Accident Considering Crack propagation during Salvage Period. Journal of Marine Science and Engineering 9(7): 737. https://doi.org/10.3390/jmse9070737

Gledić I, Parunov J, Prebeg P (2019) Low-cycle fatigue of ship hull damaged in collision. Engineering Failure Analysis 96: 436-454. https://doi.org/10.1016/j.engfailanal.2018.11.005

Hobbacher AF (2016) Recommendations for fatigue design of welded joints and components (IIW Collection; Second Edition). Switzerland, Springer

Huang W, Garbatov Y, Guedes Soares C (2014) Fatigue reliability assessment of correlated welded web-frame joints, Journal of Marine Science and Application 13(1): 23-31. https://doi. org/10.1007/s11804-014-1228-z

International Association of Classification Societies (IACS) (2014) Common Structural Rules for Bulk Carriers and Oil Tankers (IACS CSR). International Association of Classification Societies

Jovičić G, Kozak D, Milanovic V, Živković M, Živković J (2015) The influence of wagon structure part shape optimization on ultimate fatigue strength. Transactions of FAMENA 39(4): 23-35

Kodvanj J, Garbatov Y, Guedes Soares C (2021) Numerical analysis of stress concentration in non-uniformly corroded small-scale specimens. J Marine Sci Appl 20, 1-9. https://doi. org/10.1007/s11804-020-00154-2

Lassen T, Recho N (2006) Fatigue life analyses of welded structures (FLAWS). ISTE Ltd., London, United Kingdom

Parunov J, Gledić I, Garbatov Y, Guedes Soares C (2013) Fatigue Assessment of Corroded Deck Longitudinals of Tankers. International Journal of Maritime Engineering 155(A1): A9-A21. https://doi.org/10.5750/ijme.v155iA1.892

Socie DF. Morrow J, Chen WC (1979) A procedure for estimating total fatigue life of a notched and cracked members. Engineering Fracture Mechanics 11(4): 851-859. https://doi.org/10.1016/0013-7944(79)90142-5